DOI: 10.1002/ejic.201000448

Ruthenium-to-Platinum Interactions in η^6,η^1 NCN-Pincer Arene Heterobimetallic Complexes: An Experimental and Theoretical Study

Sylvestre Bonnet,[a,b] Maxime A. Siegler,[c] Joop H. van Lenthe,[d] Martin Lutz,[c] Anthony L. Spek,[c] Gerard van Koten,[a] and Robertus J. M. Klein Gebbink*[a]

Keywords: Heterometallic complexes / Ruthenium / Platinum / Density functional calculations / Arenes

A series of η^6,η^1-heterobimetallic complexes have been prepared in which a $[Ru(\eta^6\text{-arene})(C_5R_5)]^+$ fragment (R = H or Me) and an η^1-NCN-pincer platinum fragment are combined within the same molecule. In complexes $[\mathbf{2}]^+$ and $[\mathbf{3}]^+$, the ruthenium and platinum centers are η^6 and η^1 coordinated, respectively, to the same arene ring, whereas in $[\mathbf{4_A}]^+$ and $[\mathbf{5_A}]^+$ they are coordinated to two different arene rings that are linked with a covalent bond ($[\mathbf{4_A}]^+$) or an ethyl bridge ($[\mathbf{5_A}]^+$). Upon changing the organic manifold between both metal centers, very strong ($[\mathbf{2}]^+$) to very weak ($[\mathbf{5_A}]^+$) ruthenium-to-platinum interactions are obtained. Experimentally, X-ray crystal structures show an increaing steric hindrance when the Ru–Pt distance diminishes, and electrochemical and ^{195}Pt NMR spectroscopic studies show a decreasing electron density on platinum from $[\mathbf{5_A}]^+$ to $[\mathbf{2}]^+$. Theoretical DFT calculations were undertaken, which show an increasing charge on platinum from $[\mathbf{5_A}]^+$ to $[\mathbf{2}]^+$. Our theoretical analysis shows that the particularly strong ruthenium-to-platinum electronic interactions in $[\mathbf{2}]^+$ and $[\mathbf{3}]^+$ do not come from binding of ruthenium to platinum, but from the pincer C_{ipso} sharing its electron density between both metal centers, which decreases the σ donation to platinum, and from increased backdonation of the platinum d electrons into the π system of the arene ring.

Introduction

Metal-to-metal interactions represent a central topic in modern organometallic chemistry.[1–4] With short unsaturated hydrocarbon bridges metal–metal coupling can be strong, which leads to mixed-valence systems.[5,6] However, when the bridging ligand becomes longer, metal-to-metal interactions can become more elusive, hence difficult to characterize.[7,8] Most of the time, long-distance metal-to-metal interactions are transmitted through conjugated π systems like polyalkene,[9–12] polyalkyne,[13,14] or polyphenylene[15–19] ligands. Typically, both metal fragments can be connected to the bridging ligand in an axial, η^1,η^1 fashion, and interact across the organic manifold through the conjugated π system (Scheme 1, a).[18–21] Alternatively, both metal fragments can coordinate in an η^5,η^5 or η^6,η^6 fashion to the π system [i.e., perpendicularly to the axis of the organic bridge (Scheme 1, b)].[15,22] Finally, both types of binding can take place [i.e., one metal center is η^1-bonded to the bridging ligand, whereas the other is η^5- or η^6-bonded (Scheme 1, c)].[23–26]

We recently discovered[27] a straightforward route to bis-organometallic complexes of the type shown in Scheme 1c, in which the arenophile $[Ru(C_5R_5)(MeCN)_3]^+$ (R = H or Me)[15,28] directly reacts, in dichloromethane and at room temperature, with ECE-pincer platinum and palladium complexes (E = N, S, or P, see Scheme 2, a). The resulting ruthenium-modified pincer complexes show different properties compared to the starting monometallic pincer complexes: the pincer metal is more electron poor,[27] it can have an increased catalytic activity,[29] and in the event that both pincer arms are different it becomes planar-chiral.[30] However, the difference in charge introduced by the cationic ruthenium fragment questions whether the different properties of, for example, **1** and $[\mathbf{2}]^+$ (Scheme 2, a) arise from the different charges, or from intramolecular ruthenium-to-platinum interactions. As the approximately 3.9 Å ruthenium–platinum distance in complex $[\mathbf{2}]^+$ or $[\mathbf{3}]^+$ is rather short, it was also unclear whether such metal-to-metal interactions would be mediated by direct binding between ruthenium and platinum, or by the bridging ligand. Finally, the steric or electronic nature of these interactions could not be clearly established in our initial communications.

We undertook the synthesis of complexes $[\mathbf{4_A}]^+$ and $[\mathbf{5_A}]^+$ to answer these questions (Scheme 2, b). In this work,

[a] Organic Chemistry & Catalysis,
Debye Institute for Nanomaterials Science,
Faculty of Science, Utrecht University,
Padualaan 8, 3584 CH Utrecht, The Netherlands
[b] Leiden Institute of Chemistry, Gorlaeus Laboratories,
Leiden University,
PO Box 9502, 2300 RA Leiden, The Netherlands
[c] Crystal and Structural Chemistry,
Bijvoet Center for
Biomolecular Research,
Faculty of Science, Utrecht University,
Padualaan 8, 3584 CH Utrecht, The Netherlands
[d] Theoretical Chemistry Group,
Debye Institute for Nanomaterials Science,
Faculty of Science Utrecht University,
Padualaan 8, 3584 CH Utrecht, The Netherlands

Supporting information for this article is available on the WWW under http://dx.doi.org/10.1002/ejic.201000448.

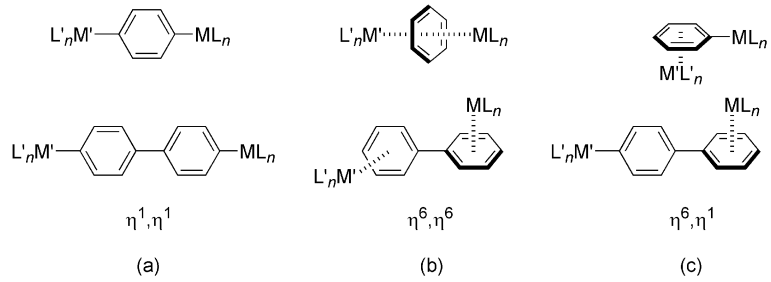

Scheme 1. Binding modes for bis-organometallic complexes bridged by a phenyl or biphenyl bridge.

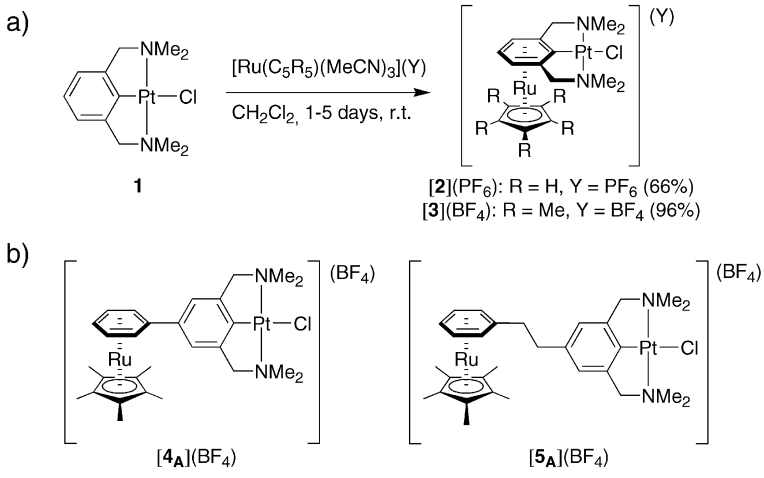

Scheme 2. η^6,η^1 NCN-pincer arene heterobimetallic complexes.

we show the synthesis of complexes $[\mathbf{4_A}]^+$ and $[\mathbf{5_A}]^+$, and compare their X-ray structures to those of **1** and $[\mathbf{3}]^+$, which gives a measure of steric effects in such η^6,η^1-bimetallic structures. In addition, electrochemical and ^{195}Pt NMR spectroscopic studies were realized, which clearly show that the low electron density on platinum in $[\mathbf{2}]^+$ and $[\mathbf{3}]^+$ is not an artifact due to the positive charge of the bimetallic complex, but the result of the electron-withdrawing influence of the ruthenium fragment on the NCN-pincer platinum moiety. DFT theoretical calculations were also undertaken to unravel the nature of ruthenium-to-platinum interactions in complexes $[\mathbf{2}]^+$ and $[\mathbf{3}]^+$. They show that there is no ruthenium–platinum bond, but rather a strong decrease of σ donation of the *ipso*-carbon atom bound to platinum, as well as increased backbonding from platinum to the π system of the arene pincer ligand due to η^6-coordination of the ruthenium atom.

Results

Synthesis and X-ray Structures

Schemes 3 and 4 describe the synthesis of Z-NCN-pincer arene ligands **7** (Z = Ph) and **9** (Z = C≡CPh), respectively, and of platinum complexes **8** and **11**. Ligands **7** and **9** were obtained, respectively, by Suzuki and Sonogashira cross-coupling reactions starting from the *para*-iodo NCN-pincer precursor **6** (Z = I).[31] The metalation conditions used for the introduction of platinum into the NCN-pincer arene ligands **7** and **9** were the same as the one used for the synthesis of **1** {i.e., lithiation at –78 °C in pentane with *n*BuLi, followed by quenching with $[PtCl_2(SEt_2)_2]$ in diethyl ether}. This procedure afforded metal complexes **8** and **10**, which had as the Z-substituent either a phenyl (**8**) or 2-phenylethynyl (**10**) group. Catalytic reduction of the alkynyl moiety in **10** under 1 atm of H_2 using Pd/C as catalyst quantitatively afforded *para*-(2-phenylethyl)-substituted NCN-pincer platinum complex **11**. Quite remarkably, the NCN-pincer platinum moiety survives these reductive conditions.

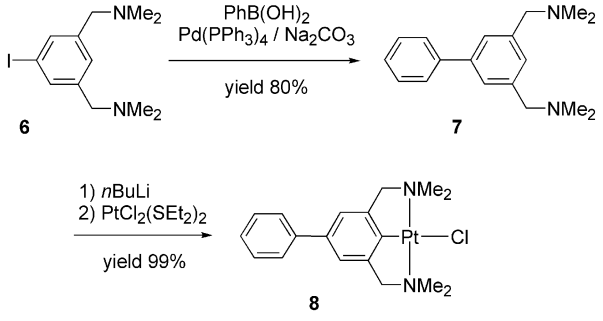

Scheme 3. Synthesis of complex **8**.

Ruthenium complexes of the type $[Ru(C_5R_5)(MeCN)_3]^+$, with R = H[28] or R = Me,[15] are known as arenophiles that react with six-membered aromatic rings to yield the corresponding $[Ru(C_5R_5)(arene)]^+$ complexes. Schemes 5

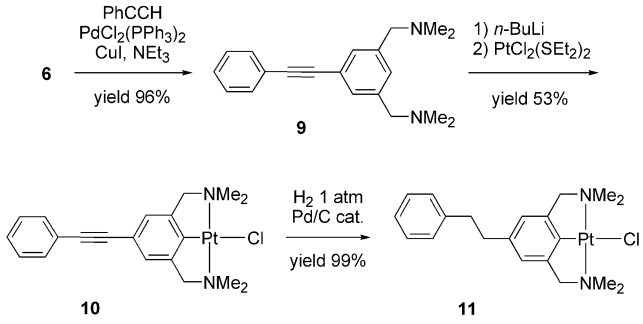

Scheme 4. Synthesis of complexes **10** and **11**.

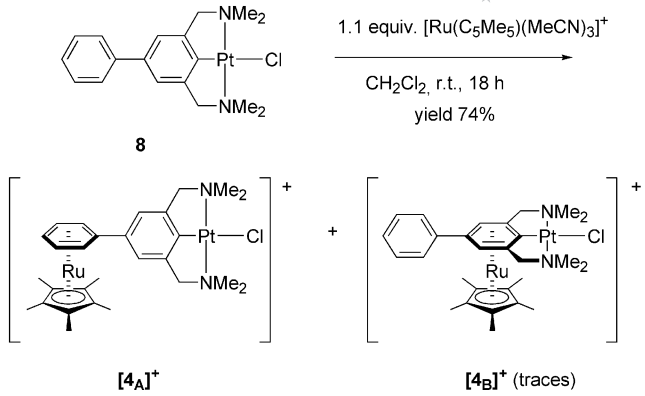

Scheme 5. Synthesis of complex $[\mathbf{4}]^+$.

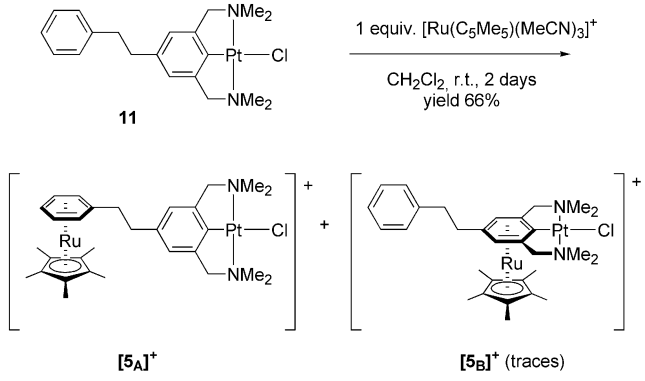

Scheme 6. Synthesis of complex $[\mathbf{5}]^+$.

and 6 show the ruthenation of NCN-pincer arene metal complexes **8** and **11**, respectively, using $[Ru(C_5Me_5)(MeCN)_3](BF_4)$ at room temperature in dichloromethane. The presence of two nonequivalent phenyl groups (i.e., one in the Z-group and one being part of the NCN-pincer system) raises selectivity issues during the η^6-coordination reactions. The two coordination isomers A and B (see Schemes 5 and 6) can be easily differentiated by ^{1}H NMR spectroscopy. High-field-shifted signals for the protons of the η^6-coordinated ring and inequivalent (diastereotopic) methylene and *N*-methyl signals are observed upon η^6-coordination to the NCN-pincer arene ring (isomers $[\mathbf{4_B}]^+$ and $[\mathbf{5_B}]^+$). In isomer $[\mathbf{4_A}]^+$ and $[\mathbf{5_A}]^+$, the protons *meta* to the carbon-to-platinum bond appear at low field ($\delta > 6.5$ ppm), whereas the three signals of the η^6-coordinated arene ring appear at higher field (between $\delta = 5.5$ and 6.5 ppm). In addition, the rotation around the C–C single bonds that separate the two arene rings is fast (low rotation barrier) at room temperature, which gives rise to singlet signals for the methylene and *N*-methyl signals (i.e., there is no facial differentiation of the pincer moiety induced by the η^6-coordinated ruthenium fragment in $[\mathbf{4_A}]^+$ and $[\mathbf{5_A}]^+$). When the less-hindered arenophile $[Ru(C_5H_5)(MeCN)_3]^+$ was used, poor selectivities were observed, and η^6-coordination reactions yielded mixtures of isomers of type A and B that could not be separated.[32] In contrast, when the more hindered reagent $[Ru(C_5Me_5)(MeCN)_3]^+$ was used, the selectivity of η^6-coordination was good and yielded isomers $[\mathbf{4_A}]^+$ and $[\mathbf{5_A}]^+$ as the major or sole product. Traces of isomer $[\mathbf{4_B}]^+$ and $[\mathbf{5_B}]^+$, observed in the crude reaction mixture by ^{1}H NMR spectroscopy, were removed during purification of the complexes. Thus, ruthenation of complexes **8** and **11** by using $[Ru(C_5Me_5)(MeCN)_3]^+$ afforded isomer A of both heterobimetallic complexes $[\mathbf{4_A}]^+$ and $[\mathbf{5_A}]^+$ in good yield. Like $[\mathbf{2}](PF_6)$ and $[\mathbf{3}](BF_4)$, complexes $[\mathbf{4_A}](BF_4)$ and $[\mathbf{5_A}](BF_4)$ have good solubility in acetone or dichloromethane, and give white solids upon precipitation from pentane. They are both very stable organometallic species because they can be handled in air for months and withstand chromatography on silica gel or alumina.

Ruthenation of alkynyl complex **10** did not allow us to isolate pure materials. Although the related compounds $[Ru(\eta^5\text{-}C_5R_5)(\eta^6\text{-}C_6H_5CCC_6H_5)]^+$ (R = H or Me) are known,[33–35] a green color appears upon addition of $[Ru(C_5Me_5)(MeCN)_3]^+$ to **10**, and purification of the η^6,η^1 product as observed by MALDI-TOF mass spectrometry (*m*/*z* calcd. for $C_{30}H_{38}ClN_2PtRu$: 758.14; found 757.96) could not be achieved.

The crystal structure of complexes $[\mathbf{4_A}]^+$ and $[\mathbf{5_A}]^+$ was determined by single-crystal X-ray diffraction (see Figure 1). Table 1 includes selected distances and angles for $[\mathbf{4_A}]^+$ and $[\mathbf{5_A}]^+$. In both complexes the typical "pincerlike" η^1-coordination of the Pt center is not violated, and the ruthenium center is η^6-coordinated to the second arene ring of the same ligand. Unlike in complex $[\mathbf{3}]^+$,[27] all Ru–C_{arene} distances in $[\mathbf{4_A}]^+$ and $[\mathbf{5_A}]^+$ are quite similar, and the planes defined by the η^6-arene ring and the Cp* ligand (η^5-C_5R_5) are nearly parallel. The typical approximate C_2 symmetry of NCN-pincer complexes is retained in complexes $[\mathbf{4_A}]^+$ and $[\mathbf{5_A}]^+$. For $[\mathbf{4_A}]^+$ there are two independent cations in the crystal with similar geometries. The biphenyl ligands are slightly twisted: the two independent torsions angles C_{13}–C_{14}–C_{113}–C_{114} [13.2(15)°] and C_{23}–C_{24}–C_{213}–C_{214} [13.0(13)°] defined between the η^1- and η^6-arene rings are the same within standard uncertainties. In the two independent cations found in the crystal for $[\mathbf{5_A}]^+$, the two arene fragments (i.e., η^6-arene···Ru···Cp* and N,C,N-pincer···Pt), which are bridged by an ethyl group, nearly adopt an *anti* conformation. The torsion angles C_{14}–C_{113}–C_{114}–C_{115} and C_{24}–C_{213}–C_{214}–C_{215} are –160.1(7) and 171.4(7)°, respectively.

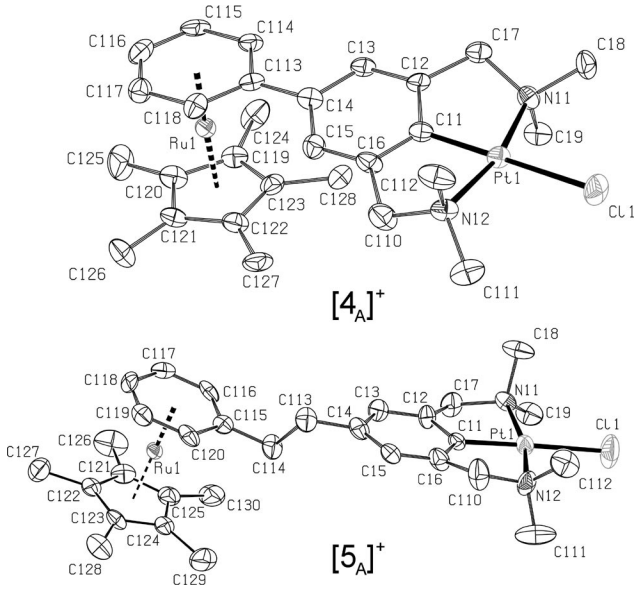

Figure 1. Displacement ellipsoid plot (drawn at the 50% probability level) of one of the two crystallographically independent cations in the asymmetric unit of $[\mathbf{4_A}]^+$ (top) and $[\mathbf{5_A}]^+$ (bottom) at 150 K. For $[\mathbf{5_A}]^+$ only the major component of the disordered Cp* ligand is shown. BF_4^- counteranions and hydrogen atoms have been omitted for clarity.

Table 1. Selected distances [Å] and angles [°] in the crystal structures of complexes $[\mathbf{4_A}](BF_4)$ and $[\mathbf{5_A}](BF_4)$.

	$[\mathbf{4_A}]^+$		$[\mathbf{5_A}]^+$	
Pt–C_{ipso}[a]	1.917(9)	1.940(9)	1.912(7)	1.926(7)
Pt–Cl	2.414(2)	2.413(2)	2.401(2)	2.4180(19)
Pt–N_1	2.105(7)	2.092(7)	2.083(6)	2.085(6)
Pt–N_2	2.101(7)	2.099(7)	2.084(7)	2.083(6)
N_1–Pt–N_2	163.6(3)	163.5(3)	165.2(3)	164.6(2)
Cl–Pt–C_{ipso}	179.5(2)	178.0(2)	178.4(2)	178.2(2)
$PtN_1N_2C_{ipso}$–$C_1C_2C_6$	11.7(13)	11.0(14)	7.1(9)	4.9(8)
Ru–C_{arene}: average	1.7109(9)	1.7106(8)	1.7090(5)	1.7064(5)
Ru–C_{arene}: shortest	2.195(7)	2.194(7)	2.201(7)	2.209(7)
Ru–C_{arene}: longest	2.236(8)	2.244(8)	2.234(11)	2.236(7)
Ru–Cp*	1.8085(9)	1.8045(7)	1.7945(5)	1.8069(5)
arene–Cp*	3.3(6)	2.5(6)	4.5(8)	2.0(4)
$C_{13}C_{14}C_{113}C_{114}$	13.1(11)	13.1(11)	10.9(3)	2.2(3)
Ru–Pt	7.6966(8)	7.5852(8)	10.2086(7)	10.2435(7)

[a] C_{ipso} is defined as the η^1-coordinated carbon atom.

Ruthenium–Platinum Interactions in Solution

^{195}Pt NMR spectroscopy and electrochemistry were used to quantify electronic interactions between the ruthenium- and platinum-containing fragments. We earlier showed[36,37] that the ^{195}Pt NMR spectroscopic signal of *para*-substituted NCN-pincer platinum complexes is linearly correlated to the Hammett constant σ_p of the *para* substituent on the arene ring, hence its ability to withdraw electrons from the metal center. Table 2 shows the ^{195}Pt NMR spectroscopic chemical shifts in dichloromethane of all platinum complexes of this study, in descending order of δ = ^{195}Pt. For monometallic platinum complexes **1**, **8**, **10**, and **11**, the ^{195}Pt NMR spectroscopic chemical shifts follow the expected *para*-substitution trends, with the triple bond in **10** acting as a slightly electron-withdrawing group, and the phenyl and alkyl substituents in **8** and **11** acting as slightly electron-donating groups. For bimetallic complexes $[\mathbf{2}]^+$, $[\mathbf{3}]^+$, $[\mathbf{4_A}]^+$, and $[\mathbf{5_A}]^+$ the ^{195}Pt NMR spectroscopic signal is low-field shifted compared to monometallic precursors, which indicates that the $[Ru(C_5R_5)]^+$ fragment has an overall electron-withdrawing effect on platinum. The strength of these effects depends on the organic manifold bridging the two metal centers. The difference in chemical shift between complexes $[\mathbf{5_A}]^+$ and **11** is very small ($\Delta\delta$ = +14 ppm). It is larger between $[\mathbf{4_A}]^+$ and **8** ($\Delta\delta$ = +60 ppm) and even larger between $[\mathbf{3}]^+$ ($\Delta\delta$ = +154 ppm) or $[\mathbf{2}]^+$ ($\Delta\delta$ = +282 ppm) and **1**. The chemical shift in $[\mathbf{2}]^+$ is significantly higher than that in the *para*-NO_2-substituted NCN-pincer platinum complex (δ = –2993 ppm),[36] thus pointing to the exceptionally low electron density of the platinum center in bimetallic complex $[\mathbf{2}]^+$.

Table 2. ^{195}Pt NMR spectroscopic chemical shifts (δ) and oxidation potential as determined by cyclic voltammetry for arene-pincer platinum complexes. The table is sorted by increasing values of δ.

Complex	δ [ppm][a]	$E_{ox}(Pt^{II}/Pt^{IV})$ [V][b]
11	–3199	+0.53
$[\mathbf{5_A}]^+$	–3185	+0.59
8	–3171	+0.58
1	–3150	+0.65
10	–3137	+0.63
$[\mathbf{4_A}]^+$	–3111	+0.80
$[\mathbf{3}]^+$	–2996	+1.15
$[\mathbf{2}]^+$	–2868	+1.24

[a] In CD_2Cl_2, using Na_2PtCl_6 in D_2O as an external reference. [b] In CH_3CN, NBu_4PF_6 0.1 M, platinum electrode, scan rate: 100 mV s^{-1}, at 298 K (Pt^{II}/Pt^{IV} oxidation is electrochemically irreversible in all cases).

Cyclic voltammetry in acetonitrile showed, for each NCN-pincer platinum-containing complex, an electrochemically irreversible oxidation wave, which was shown to correspond to a $Pt^{II} \rightarrow Pt^{IV}$ oxidation.[38–40] These oxidation potentials are also reported in Table 2. Although the measured oxidation potentials do not correspond to an electrochemically reversible process, their evolution fully confirms the trends observed by ^{195}Pt NMR spectroscopy. There is a small shift (ΔE = 60 mV) between $[\mathbf{5_A}]^+$ and **11**, a larger shift between $[\mathbf{4_A}]^+$ and **8** (ΔE = 220 mV), and the largest shift between $[\mathbf{3}]^+$ (ΔE = 500 mV) or $[\mathbf{2}]^+$ (ΔE = 590 mV) and **1**, thereby showing the electron-withdrawing effects of the ruthenium fragment on platinum.

Quantum Calculations

To model the electronic interactions observed in solution, we undertook DFT calculations using B3LYP/LANL2DZ as implemented in the GAMESS-UK program.[41] The structures of **1**,[42] **[2]**(Cl), **[3]**(Cl), $[\mathbf{4_A}]$(Cl), and $[\mathbf{5_A}]$(Cl) were minimized by using chloride as a counteranion for the cationic complexes (see Figure S5 in the Supporting Information). The computed structures were found to be very similar to the available X-ray structures.[36] For each computed structure, natural charges (Q) were computed accord-

ing to the natural bond orbital (NBO) analysis,[43] as well as bond indices (BI),[44] Mulliken overlap populations,[45] and the total dipole moment of the NCN-pincer platinum-containing fragment (see Table 3). The energy $E_{Ptd_{z^2}}$ of the occupied molecular orbital of d_{z^2} character centered on platinum, as well as the energy E_σ of the highest occupied molecular orbital (HOMO) of σ type for the Pt–C_{ipso} bond, is also reported.

Table 3. DFT-calculated parameters for complexes **1** and [**2**](Cl) to [$\mathbf{5_A}$](Cl). Distances are given in Å; natural charges (*Q*), Mulliken overlap populations (MOP), and bond indexes (BI) in atomic units; energies (*E*) in eV; and dipole moments in debye. The table is ordered according to increasing values of *Q*(Pt).

Complexes	**1**	[$\mathbf{5_A}$](Cl)	[$\mathbf{4_A}$](Cl)	[**3**](Cl)	[**2**](Cl)
Q(Pt)	0.565	0.569	0.578	0.598	0.603
Q(C_{ipso})	–0.220	–0.223	–0.213	–0.225	–0.220
Q(Ru)	–	0.115	0.121	0.120	0.144
BI(Pt–C_{ipso})	0.823	0.838	0.846	0.658	0.696
d(Pt–C_{ipso}) [Å]	1.944	1.940	1.936	1.930	1.927
MOP(Pt–C_{ipso})	0.144	0.135	0.123	–0.303	–0.240
BI(Ru–C_{ipso})[a]	–	0.294	0.283	0.296	0.300
d(Ru–C_{ipso}) [Å][a]	–	2.358	2.382	2.406	2.385
BI(Ru–Pt)	–	0.000	0.004	0.048	0.047
d(Ru–Pt)	–	10.012	8.072	4.059	3.929
$E_{Ptd_{z^2}}$ [eV]	–5.85	–6.16	–6.40	–6.63	–6.59
E_σ [eV][b]	–6.57	–6.85	–7.07	–7.52	–7.20
Dipole moment [D][d]	5.12	26.7[c]	19.6[c]	11.0[c]	10.8[c]

[a] Mulliken overlap population. [b] In [$\mathbf{4_A}$](Cl), and [$\mathbf{5_A}$](Cl), C_{ipso} and C_{para} are defined as belonging to the η^6-coordinated arene ring and in *ipso*- or *para*-position, respectively, to the NCN-pincer substituent. [c] The corresponding orbitals are HOMO–5, HOMO–9, HOMO–11, HOMO–12, and HOMO–8 for complexes **1**, [$\mathbf{5_A}$](Cl), [$\mathbf{4_A}$](Cl), [**3**](Cl), and [**2**](Cl), respectively. [d] Calculated for the cationic part of the bimetallic complexes (i.e., after removal of the chloride counteranion).

According to these calculations, moving along the series **1**, [$\mathbf{5_A}$](Cl), [$\mathbf{4_A}$](Cl), [**3**](Cl), and [**2**](Cl) leads to the following observations: (1) the positive NBO charges *Q*(Pt) and *Q*(Ru) on both metal centers increase; (2) the energy level $E_{Ptd_{z^2}}$ decreases; (3) the negative NBO charge on the chloride ligand decreases; and (4) the carbon-to-platinum distance *d*(C_{ipso}–Pt) decreases, although the corresponding bond index is much lower in [**2**](Cl) and [**3**](Cl) than in **1**, [$\mathbf{4_A}$](Cl), and [$\mathbf{5_A}$](Cl). Although these changes occur, the charge on C_{ipso} remains constant, as well as the bond index and the distance between the ruthenium center and the carbon atoms of the η^6-coordinated arene ring. In all bimetallic complexes, including [**2**](Cl) and [**3**](Cl), the bond index between the ruthenium and platinum atoms remains very low (<0.05), which is usually interpreted as an absence of direct chemical bonding between the two metal centers.[46]

Discussion

The synthetic method for complexes $[\mathbf{4_A}]^+$ and $[\mathbf{5_A}]^+$ follows the methodology described for $[\mathbf{2}]^+$ and $[\mathbf{3}]^+$: introduction of the carbon-to-platinum bond is realized first, followed by η^6-complexation of the $[Ru(C_5Me_5)]^+$ organometallic fragment. In the few cases in which η^6-coordination of $[Ru(C_5Me_5)]^+$ was reported for molecules bearing non-equivalent phenyl groups, discrimination between the different arene coordination sites was achieved by playing on steric and/or electronic effects.[47] Wheeler et al.[48] have mentioned that η^6-coordination of $[Ru(C_5Me_5)(MeCN)_3]^+$ is largely controlled by steric factors, and that when steric hindrance is small, electronic factors are also important. In complexes **8** and **11**, both arene rings are electron-rich,[49] but the σ-metallated arene ring is more electron-rich than the other due to the partial negative charge on the *ipso*-carbon atom. When the less-hindered electrophile $[Ru(C_5H_5)(MeCN)_3]^+$ is used, bad selectivities are observed and a mixture of isomers A and B is obtained (see Schemes 5 and 6). In contrast, when the more hindered electrophile $[Ru(C_5Me_5)(MeCN)_3]^+$ is used, η^6-coordination occurs preferentially to the pendant phenyl group if present (isomer A), thus yielding a crude product that contains only traces of isomer B. If no pendant phenyl group is available like in complex **1**, η^6-coordination does occur to the arene ring of the pincer itself to give complexes $[\mathbf{2}]^+$ and $[\mathbf{3}]^+$.[27] We interpret such reactivity pattern as a sign of limited steric congestion between the $[Ru(C_5Me_5)]^+$ fragment and the *N*-methyl groups of the NCN-pincer metal moiety. This steric hindrance is low enough to allow the synthesis of complexes $[\mathbf{2}]^+$ and $[\mathbf{3}]^+$ in good yields but high enough to yield selectively the isomer A of complexes $[\mathbf{4_A}]^+$ and $[\mathbf{5_A}]^+$.

Complexes $[\mathbf{4_A}]^+$ and $[\mathbf{5_A}]^+$ share many characteristics with $[\mathbf{3}]^+$,[27] namely, the combination of η^6-coordination to $[Ru(C_5Me_5)]^+$ and η^1-coordination to $[PtCl]^+$, the NCN-pincer terdentate framework, the positive global charge, and the BF_4^- counteranions (see Table 1 and Figure 2). The X-ray structure of complex $[Ru(C_5Me_5)(\eta^6\text{-}1,3\text{-}(Me_2NCH_2)_2\text{-}C_6H_4)](BF_4)$, noted [**12**]($BF_4$), has been published elsewhere.[50] Complexes **1**[51] and $[\mathbf{12}]^+$ are good reference compounds, as they bear only one of the two metal centers found in the bimetallic complexes $[\mathbf{3}]^+$–$[\mathbf{5_A}]^+$. Table S1 (see the Supporting Information) shows the main geometrical parameters for complexes **1**, $[\mathbf{3}]^+$, and $[\mathbf{12}]^+$, to be compared with Table 1.

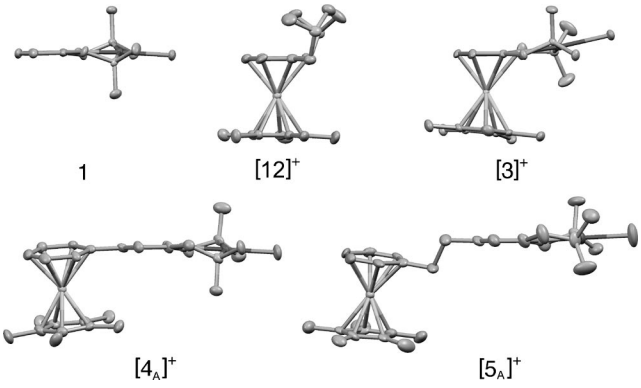

Figure 2. Side view of the geometry observed in the solid state (X-rays) for monometallic complexes **1**,[51] $[\mathbf{12}]^+$,[50] and bimetallic complexes $[\mathbf{3}]^+$,[27] $[\mathbf{4_A}]^+$, and $[\mathbf{5_A}]^+$. For $[\mathbf{12}]^+$, $[\mathbf{4_A}]^+$, and $[\mathbf{5_A}]^+$, only one of the different geometries found in the unit cell is shown (i.e., that which contains Ru1). Hydrogen atoms and BF_4^- counteranions have been omitted for clarity.

In the solid state, several geometrical features of complexes $[3]^+$, $[4_A]^+$, and $[5_A]^+$ are similar to that found for complex **1**: (1) the square-planar geometry around platinum is distorted, since the bond angles N–Pt–N and Cl–Pt–C_{ipso} are significantly smaller than 180°; (2) the conformations of the five-membered metallacycles including the platinum center are puckered, with the dihedral angles defined between the Pt–C_{ipso}–N_1–N_2 and C_{ipso}–C_2–C_6 planes being significantly larger in **1** and smaller in $[5_A]^+$; and (3) the presence of the ruthenium fragment in complexes $[3]^+$–$[5_A]^+$ has no significant effect on the bond lengths Pt–C_{ipso}, Pt–N, and Pt–Cl.

However, noticeable differences in the crystal structures shown in Figure 2 are observed as follows:

(i) Going from $[3]^+$ to $[5_A]^+$, the intramolecular distances between the ruthenium and platinum atoms increase, from 3.9320(3) Å in $[3]^+$ to 7.5856(8) and 7.6968(8) Å in $[4_A]^+$, and up to 10.2086(7) and 10.2435(7) Å in $[5_A]^+$.

(ii) The distances between the ruthenium center and the average plane of the η^6-coordinated arene ring gradually increase when going down the series $[12]^+ < [5_A]^+ < [4_A]^+ < [3]^+$.

(iii) The difference Δd(Ru–C) between the longest and the shortest Ru–C bond lengths, in which C belongs to the η^6-coordinated arene ring, increases following the series $[12]^+ < [5_A]^+ < [4_A]^+ < [3]^+$ {Δd(Ru–C) = 0. 023(10) Å for $[12]^+$, 0.027(10) and 0.033(13) Å for $[5_A]^+$, 0.041(11) and 0.050(10) Å for $[4_A]^+$, and 0.116(3) Å for $[3]^+$}. Such differences are due to the tilting of the η^6-coordinated arene ring compared to the cyclopentadienyl ring. This tilting is large in the most hindered compound $[3]^+$, intermediate in complexes $[4_A]^+$ and $[5_A]^+$, and small in the least-hindered, platinum-free compound $[12]^+$.

(iv) In $[12]^+$ there is no platinum center. As a result, the N atoms of the amine arms are not coordinated and point opposite to the ruthenium fragment with respect to the arene ring.[50]

We interpret points (ii) and (iii) as structural signs of intramolecular steric hindrance between the methyl groups of the [(η^6-arene)RuCp*]$^+$ fragment and the NCN-pincer moiety, which increases following the series $[12]^+$, $[5_A]^+$, $[4_A]^+$, $[3]^+$. In the case of $[3]^+$, the *N*-methyl groups directly interact with the Cp* ligand, which induces distortions in the molecular geometry. These steric interactions consistently explain the regioselectivity observed in the reaction between $[Ru(C_5Me_5)(MeCN)_3]^+$ and **8** or **11**, in which the most hindered isomer (B) of complexes $[4]^+$ and $[5]^+$ is not formed.

We have earlier established that the NCN-pincer platinum fragment is an electron-rich moiety.[49] Considering the positive charge of the ruthenium fragment, we calculated the dipole moment for cations $[2]^+$–$[5_A]^+$ by DFT: as shown in Table 3, for $[2]^+$ and $[3]^+$ it is twice as large as for **1**, four times as large for $[4_A]^+$ (20 debye), and for $[5_A]^+$ it is the largest of all (27 debye in the *trans* conformation of the ethyl bridge). As shown in Figure 3, there is a good correlation between the Ru–Pt distance measured in the X-ray crystal structures of $[3]^+$–$[5_A]^+$ and the theoretical dipole moments of the cations $[3]^+$–$[5_A]^+$ as calculated by DFT. This correlation implies that in spite of the donor–acceptor nature of bimetallic complexes $[3]^+$–$[5_A]^+$, the [RuCp*(η^6-arene)]$^+$ fragment remains globally electron-deficient and the NCN-pincer platinum fragment globally electron-rich. Thus, a dipole is generated, rather than a mixed-valence complex. Analysis of the packing in the X-ray structures of $[4_A]^+$, and $[5_A]^+$ (see Figure 4 and the Supporting Information) shows that the bimetallic cations arrange in a head-to-tail fashion in the solid state, with the electron-rich platinum fragment facing the electron-poor ruthenium fragment of a neighboring cation. These "dimers" can be interpreted as resulting from the dipole moment of the cations, the antiparallel assembly of which probably helps to minimize the total energy of the crystal. This type of "dimer" is not present in the X-ray structure of complex $[3]^+$,[27] possibly because in $[3]^+$ the dipole moment of the cation is not large enough.

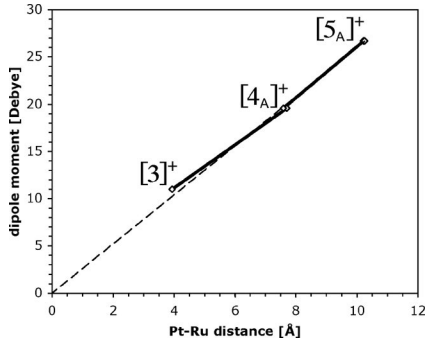

Figure 3. Correlation between the Ru–Pt distance observed in the X-ray structure of $[3](BF_4)\cdot CH_2Cl_2$, $[4_A](BF_4)$, and $[5_A](BF_4)$, and the dipole moment of the cation for the DFT-minimized structures of [3](Cl)–[5_A](Cl).

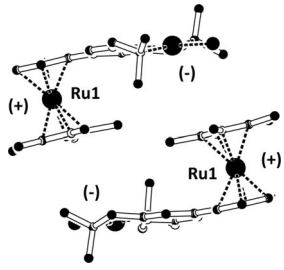

Figure 4. Dimers of cations $[4]^+$ viewed down the [–1 1 0] direction. Positive (+) and negative (–) charges symbolize the partial charge carried by the electron-poor ruthenium(arene) fragment, and the electron-rich NCN-pincer platinum moiety, respectively. BF_4^- counteranions and hydrogen atoms have been omitted for clarity. See also Figure S2 in the Supporting Information.

^{195}Pt NMR spectroscopic studies show that the electron density on platinum is decreased down the series $[5_A]^+$, $[4_A]^+$, $[3]^+$, $[2]^+$.[52] According to electrochemical data such reduced electron density is correlated with an increase of the oxidation potentials [see $E_{ox}(Pt^{II}/Pt^{IV})$ in Table 2], which confirms that the oxidations are platinum-based. Qualitatively, four parameters can explain these evolutions. First, the saturated alkane bridge in $[5_A]^+$ prevents any con-

jugation between the η^6-coordinated and η^1-coordinated arene rings. In complex $[\mathbf{4_A}]^+$, conjugation between the η^6- and η^1-coordinated arene rings is possible but limited (in solution) by the rotation of the two rings around the central C–C σ bond. By contrast, in $[\mathbf{3}]^+$ the coordination geometry is rigid and the two metals are addressing the electrons of one and the same arene ring, which leads to strong electronic interactions. Finally, the Cp ligand is less electron-rich than Cp*, thus making the $[Ru(C_5H_5)]^+$ fragment in $[\mathbf{2}]^+$ more electron-withdrawing than $[Ru(C_5Me_5)]^+$ in $[\mathbf{3}]^+$.

DFT calculations give a more quantitative analysis of the ruthenium-to-platinum electronic interactions in complexes [**2**](Cl)–[$\mathbf{5_A}$](Cl). First, as the bond index between Pt and Ru in all bimetallic complexes is very low (<0.05), direct binding of ruthenium to platinum can be ruled out. As a consequence, ruthenium-to-platinum interactions are mediated through the ligand. Second, as the Pt–C_{ipso} bond index is significantly weaker in [**2**](Cl) and [**3**](Cl) than in **1** (see Table 3), η^6-coordination of ruthenium affects the primary interaction between $[PtCl]^+$ and the $[NCN]^-$ anion. The Mulliken group population analysis shows that the overlap population between Pt and C_{ipso} is positive in **1**, [**4**](Cl), and [**5**](Cl), whereas it is negative in [**2**](Cl) and [**3**](Cl) (see Table 3). Thus, according to Mulliken[45] the platinum atom is essentially bonded to C_{ipso} in the former group, whereas there is more backbonding in the latter.

In a purely covalent approach, the Pt–C_{ipso} bond in complex **1** is a σ bond, which results primarily from the donation of the $HOMO^{[NCN]}$ of the $[NCN]^-$ fragment into the $LUMO^{[PtCl]}$ of the $[PtCl]^+$ fragment. The best representation of this interaction is the [**1**]HOMO-5 molecular orbital of **1**, which is shown in part a of Figure 5 (E_σ = –7.20 eV, see Table 3). The π* orbitals of the conjugated arene system are too high in energy in **1** to contribute significantly to backbonding. The overall result of σ binding is a large transfer of electron density from the NCN-pincer anionic ligand to the platinum atom, the positive charge of which is much lower [Q(Pt) = +0.565] in **1** than in $[PtCl]^+$ [Q(Pt) = +1.07]. Similarly, in [$\mathbf{4_A}$](Cl) and [$\mathbf{5_A}$](Cl) the molecular orbital corresponding to the Pt–C_{ipso} σ bond has no contribution from the ruthenium atom (see Figure 5, b), and the positive Mulliken overlap population is consistent with negligible backbonding from Pt to C_{ipso}. The energy E_σ of the σ Pt–C_{ipso} molecular orbital appears at slightly lower values in these complexes compared to **1** (–7.07 and –6.85 eV, respectively, see Table 3) due to the inductive effects of, respectively, the *para*-$[Ru(C_5Me_5)(C_6H_5)]^+$ and *para*-$[Ru(C_5Me_5)(C_6H_5C_2H_4)]^+$ substituents.

In [**2**](Cl) and [**3**](Cl), the [**2**]HOMO–8 and [**3**]HOMO–12 molecular orbitals that represent the donation of the NCN-pincer ligand into platinum, respectively, show a significant contribution from a ruthenium-centered $d_{z^2-x^2}$ atomic orbital (see Figure 5, c). Such mixing between atomic orbitals of σ and π character is allowed because the C_2 symmetry of the pincer fragment is broken by η^6-coordination. Thus, the contribution of ruthenium-centered d orbitals in the binding combination of the Pt–C_{ipso} σ bond lowers its energy by increased delocalization (see Table 3). It also reduces σ donation from the NCN-pincer ligand to the Pt atom, as the electron density borne by C_{ipso} is shared between the two metal centers. Meanwhile, the binding interactions between the arene ring and the ruthenium atom considerably lower the energy of the arene π* orbitals, so that they can also interact with the filled, platinum-centered d orbitals (see Figure 5, d). Backbonding from platinum into the π* system of the η^6,η^1-coordinated phenyl ring is significant in [**2**](Cl) and [**3**](Cl). Reduced σ donation and increased π backdonation both contribute to an increase in the positive charge on platinum in complexes [**2**](Cl) and [**3**](Cl), compared to **1**, [**4**](Cl), and [**5**](Cl). Thus, the particularly low electron density on platinum in complexes [**2**](Cl) and [**3**](Cl) is neither a consequence of the positive charge of the bimetallic complexes, nor of direct platinum–ruthenium binding, rather it comes from the strong modification of the character of the Pt–C_{ipso} bond that is induced by the nearby η^6-coordinated ruthenium atom.

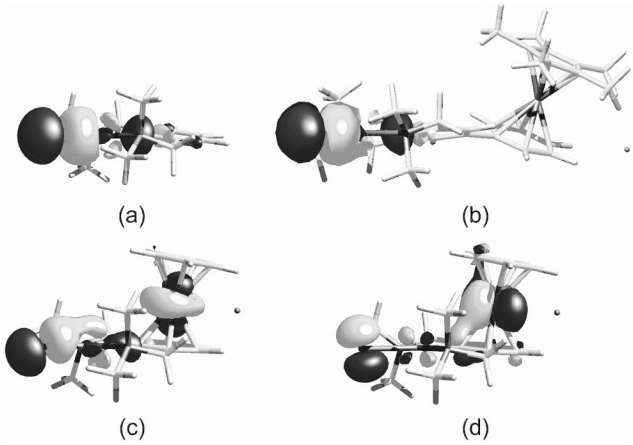

Figure 5. Representative molecular orbitals (see text); (a) [**1**]-HOMO–5 for complex **1**; (b) [**4**]HOMO–11 for complex [**4**](Cl); (c) [**2**]HOMO–8 for complex [**2**](Cl); (d) [**2**]HOMO–7 for complex [**2**](Cl).

Conclusion

We have synthesized a series of bimetallic complexes $[\mathbf{5_A}]^+$, $[\mathbf{4_A}]^+$, $[\mathbf{3}]^+$, and $[\mathbf{2}]^+$ with decreasing electron richness of the platinum center. DFT calculations show that none of these η^6,η^1 complexes have direct binding of ruthenium to platinum through space, but that the electronic interactions are mediated through the bridging ligand. When the η^6- and η^1-bonded metals are coordinated to two different arene rings as in $[\mathbf{4_A}]^+$ and $[\mathbf{5_A}]^+$, the decrease in electron density on platinum is limited, but the large intermetallic distance induces a high dipole moment in the ground state, which leads to dimerization in the solid state. By contrast, the dipole moment of $[\mathbf{2}]^+$ and $[\mathbf{3}]^+$ is much smaller, but the electron density on platinum is especially low due to the specific coordination pattern of the η^6,η^1-coordinated phenyl ring. When the two metals are coordinated to the same arene ring indeed, the σ character of the Pt–C_{ipso} bond decreases and backbonding increases relative to $[\mathbf{4_A}]^+$

and $[\mathbf{5}_A]^+$. We already noticed[27] that for complexes $[\mathbf{2}]^+$ and $[\mathbf{3}]^+$ the decreased electron density on platinum diminishes its nucleophilicity towards small electrophiles like SO_2 and I_2; the π acidity of these new complexes will also be interesting to study, as they might lead to new catalytic properties.[53]

Experimental Section

General: All reactions using sensitive reagents were performed under an atmosphere of dinitrogen using Schlenk techniques. THF and Et_2O were dried with Na/benzophenone. MeCN and CH_2Cl_2 were dried with CaH_2, and all solvents were freshly distilled under nitrogen prior to use. ^1H (300.1/400.0 MHz) and ^{13}C (75.5/100.6 MHz) NMR spectra were recorded with a Varian INOVA 300 or 400 MHz spectrometer; $^{31}P\{^1H\}$ (121.5 MHz) and ^{19}F (376 MHz) NMR spectra were recorded with a Varian INOVA 400 MHz spectrometer; and ^{195}Pt (64.5 MHz) NMR spectra were recorded with a Varian INOVA 300 MHz spectrometer. Chemical-shift values are reported in ppm (δ) relative to Me_4Si (^1H and ^{13}C NMR spectroscopy) or an NMR spectroscopy tube that contained Na_2PtCl_6 in D_2O (as external reference). MS measurements were carried out with an Applied Biosystems Voyager DE-STR MALDI-TOF mass spectrometer. Elemental analyses were performed by H. Kolbe Microanalysis Laboratories, Mülheim, Germany. For column chromatography, Merck silica gel 60 (230–400 mesh) was used. All standards reagents were purchased from Acros Organics and Aldrich Chemical Co. Inc, and used as received. $[Ru(C_5H_5)(MeCN)_3](PF_6)$[28] and $[Ru(C_5Me_5)(MeCN)_3](PF_6)$[15] were prepared according to the literature, stored and weighed under dinitrogen at room temperature in a glove box. Z-NCN pincer ligands (Z = *para*-substituent; **6**: Z = I;[31] **7**: Z = Ph[54]), NCN-pincer complex [PtCl(Z-NCN)] (**1**: Z = H),[55] and their ruthenated derivatives $[\mathbf{2}](PF_6)$ and $[\mathbf{3}](BF_4)$[27] were prepared according to literature procedures. 1,3-$(Me_2NCH_2)_2C_6H_4$ was prepared as follows: α,α′-dibromoxylene (5 g, 19 mmol) was dissolved in dichloromethane (100 mL) and cooled to 0 °C. Anhydrous dimethylamine (12 mL, 181 mmol) was added under strong stirring, the cooling bath removed, and the solution stirred under air at room temperature for 3 h. The organic layer was washed with water, brine, dried with $MgSO_4$, and the solvents evaporated. Flash distillation of the crude yellowish oil afforded a colorless, smelly liquid (2.9 g, 80%). Analytical data have been published elsewhere.[56]

Compound 8: *n*BuLi (1.4 mL, 2.2 mmol) was added to a solution of the ligand **7** (601 mg, 2.2 mmol) in dry pentane (20 mL) at –78 °C. After the addition was completed, the temperature was allowed to rise to room temperature and stirring was continued for 16 h. Subsequently, pentane was evaporated and replaced by dry ethyl ether (20 mL), then $[PtCl_2(SEt_2)_2]$ (999 mg, 2.2 mmol) was added as a solid under a flow of nitrogen, and the resulting suspension was stirred at room temperature for 24 h. Technical-grade diethyl ether was added, the suspension centrifuged, the ethereal layer decanted, and the crude solid reprecipitated from dichloromethane and pentane to afford 769 mg of a colored product. Filtration over alumina (CH_2Cl_2 as eluent) afforded **8** (542 mg, 50%) as a white powder. ^1H NMR (400 MHz, CD_2Cl_2): δ = 7.55 (d, J = 7.1, 1.4 Hz, 2 H, o′), 7.41 (t, J = 5.4, 1.8 Hz, 2 H, m′), 7.31 (t, J = 7.2, 1.3 Hz, 1 H, p′), 7.06 (s, 2 H, m), 4.09 (s, $J_{H,Pt}$ = 22.5 Hz, 4 H, CH_2N), 3.08 (s, $J_{H,Pt}$ = 18.3 Hz, 12 H, NMe_2) ppm. ^{13}C NMR (75 MHz, in CD_2Cl_2): δ = 144.8 (o), 143.8 (i), 142.0 (i′), 136.1 (p′), 128.4 (o′ + p′), 126.1 (m′), 117.9 (m, $J_{C,Pt}$ = 18.4 Hz), 77.3 ($J_{C,Pt}$ = 31.4 Hz, CH_2N), 53.9 (NMe_2) ppm. ^{195}Pt NMR (64.5 MHz, CD_2Cl_2): δ = –3171.8 ppm. MALDI-TOF: *m*/*z* calcd. for **8** $[M - PtCl]^+$ 267.2; found 267.5; *m*/*z* calcd. for **8** $[M - Cl]^+$ 462.15; found 461.5; calcd. C 43.42, H 4.66, N 5.63; found C 43.48, H 4.72, N 5.56. UV/Vis spectroscopy (ε, $L\,mol^{-1}\,cm^{-1}$): λ = 304 (22100) nm.

Compound 9: Precursor **6**[31] (3.14 g, 9.9 mmol) was weighed in a dry round-bottomed flask and put under an inert atmosphere. Degassed triethylamine (70 mL), CuI (19 mg, 0.099 mmol), $[PdCl_2(PPh_3)_2]$ (70 mg, 0.099 mmol), and phenylacetylene (1.15 mL, 10.5 mmol) were subsequently added to the reaction flask, which was stirred under dinitrogen for 2 h at room temperature. After evaporation of triethylamine, $NaHCO_3$ (100 mL) was added and the product was extracted three times with ethyl ether, washed with water, dried with $MgSO_4$, and the solvents evaporated. The crude product (3.3 g) was purified by chromatography on alumina using an 80:20:1 mixture (v/v) of pentane/dichloromethane/triethylamine. The main fraction contained 2.76 g of analytically pure product (96%). ^1H NMR (400 MHz, $CDCl_3$): δ = 7.52 (d, J = 8.0 Hz, 2 H, o′), 7.42 (s, 2 H, m), 7.33 (m, 3 H, m′ + p′), 3.42 (s, 4 H, CH_2N), 2.26 (s, 12 H, NMe_2) ppm. ^{13}C NMR (100 MHz, $CDCl_3$): δ = 139.4, 131.7, 131.1, 130.0, 128.5, 128.3, 123.5 and 123.2 (arom), 89.7 and 89.3 (C≡C), 64.1 (CH_2N), 45.6 (NMe_2) ppm. MALDI-TOF: *m*/*z* calcd. for **9** $[M + H]^+$ 293.20; found 293.49; calcd. C 82.15, H 8.27, N 9.58; found C 82.26, H 8.21, N 9.52.

Compound 10: Ligand **9** (1.0 g, 3.42 mmol) was weighed in a flame-dried Schlenk flask and put under a nitrogen atmosphere. Dry pentane (20 mL) was added, and the solution was cooled down to –78 °C. *n*BuLi (2.2 mL, 3.5 mmol) was added dropwise to give an orange solution, which was stirred at –78 °C for 30 min. The cooling bath was then removed, and the solution warmed up to room temperature overnight (18 h) to yield a yellowish suspension. Pentane was evaporated and replaced by dry ethyl ether (50 mL), then $[PtCl_2(SEt_2)_2]$ (1.53 g, 3.42 mmol) was added under a flow of dinitrogen. The yellow suspension was stirred overnight at room temperature (20 h), centrifuged, and the ethereal phase removed by decantation. The remaining solid was dissolved in dichloromethane, precipitated with pentane, centrifuged, and decanted to afford 1.41 g of a colored solid. Filtration with alumina using dichloromethane as the eluent afforded the analytically pure complex **10** (942 mg, 53%). ^1H NMR (300 MHz, CD_2Cl_2): δ = 7.49 (m, 2 H, o′), 7.33 (m, 3 H, m′ + p′), 6.99 (s, 2 H, m), 4.02 (s, $J_{H,Pt}$ = 23.1 Hz, 4 H, CH_2N), 3.03 (s, $J_{H,Pt}$ = 19.0 Hz, 12 H, NMe_2) ppm. ^{13}C NMR (75 MHz, CD_2Cl_2): δ = 148.1 (*ipso*), 144.1 (o), 131.5 (p′), 128.8 (m′), 128.2 (o′), 124.1 (i′), 122.7 (m), 117.4 (p), 87.8 (C≡C), 77.7 (CH_2N), 54.5 (NMe_2) ppm. ^{195}Pt NMR (64.5 MHz, ,in CD_2Cl_2): δ = –3136.6 ppm. MALDI-TOF: *m*/*z* calcd. for **10** $[M - PtCl]^+$ 291.41; found 291.34; *m*/*z* calcd. for **10** $[M - Cl]^+$ 486.15; found 486.29; *m*/*z* calcd. for **10** $[2M - Cl]^+$ 1007.27; found 1007.20; calcd. C 46.02, H 4.44, N 5.37; found C 45.91, H 4.53, N 5.27.

Compound 11: The alkyne complex **10** (200 mg, 383 μmol) was dissolved in technical-grade dichloromethane (100 mL). Pd/C (40 mg, 10% w/w) was added, and the mixture vigorously stirred under of dihydrogen (1 atm) at room temperature for 24 h. The black suspension was filtered through Celite and the solvent evaporated to yield the fully hydrogenated product **11** (200 mg, 99%). ^1H NMR (400 MHz, CD_2Cl_2): δ = 7.28 (m, 2 H, o′), 7.22 (m, 3 H, m′ + p′), 7.68 (s, 2 H, m), 3.99 (s, $J_{H,Pt}$ = 22.5 Hz, 4 H, CH_2N), 3.04 (s, $J_{H,Pt}$ = 17.5 Hz, 12 H, NMe_2), 2.88 (m, 2 H, CH_2^{α}), 2.76 (m, 2 H, CH_2^{β}) ppm. ^{13}C NMR (75 MHz, CD_2Cl_2): δ = 143.8 (o), 142.8 (*ipso*), 142.5 (i′), 137.2 (p′), 128.7 (m′), 128.6 (o′), 126.1 (p), 119.6 (m, $J_{C,Pt}$ = 17.8 Hz), 78.1 ($J_{C,Pt}$ = 32.6 Hz, CH_2N), 54.6 (NMe_2), 38.8

EurJIC European Journal of Inorganic Chemistry

(CH_2), 38.6 (CH_2') ppm. ^{195}Pt NMR (64.5 MHz, CD_2Cl_2): δ = –3198.6 ppm. MALDI-TOF: *m*/*z* calcd. for **11** [M – PtCl]$^+$ 295.22; found 295.39; *m*/*z* calcd. for **11** [M – Cl]$^+$ 490.18; found 490.39; *m*/*z* calcd. for **11** [M]$^+$ = 525.15; found 525.31; *m*/*z* calcd. for **11** [2M – Cl]$^+$ 1014.3; found 1015.3; calcd. C 45.75, H 5.24, N 6.32; found C 45.67, H 5.17, N 5.33.

Compound [4$_A$](BF$_4$): Complex **8** (100 mg, 201 μmol) was weighed in a dry Schlenk flask and put under inert atmosphere. A solution of [RuCp*(MeCN)$_3$](BF$_4$) (103 mg, 230 μmol) in dry dichloromethane (5 mL) was added, and the mixture stirred under nitrogen at room temperature for 18 h. The crude solution ([**4**$_A$]$^+$/[**4**$_B$]$^+$ = 37:1 by ^{1}H NMR spectroscopy) was put on top of a 50 mL alumina column and eluted with CH_2Cl_2 that contained 1% (v/v) methanol. Yield: 122 mg of [**4**$_A$](BF$_4$) as a whitish powder (74%). ^{1}H NMR (400 MHz, CD_2Cl_2): δ = 7.07 (s, 2 H, m), 6.21 (d, *J* = 6.2 Hz, 2 H, o′), 5.88 (t, *J* = 5.9 Hz, 2 H, m′), 5.77 (t, *J* = 5.7 Hz, 1 H, p′), 4.20 (s, $J_{H,Pt}$ = 21.8 Hz, 4 H, CH_2N), 2.92 (s, $J_{H,Pt}$ = 17.4 Hz, 12 H, NMe_2), 1.89 (s, 15 H, C_5Me_5) ppm. ^{13}C NMR (75 MHz, CD_2Cl_2): δ = 149.7 (i), 144.5 (o), 126.0 (p), 117.6 (m, $J_{C,Pt}$ = 17.3 Hz), 103.5 (i′), 95.8 (C_5R_5), 86.6, 86.1, 83.5 (o′, m′, p′), 76.9 ($J_{C,Pt}$ = 31.4 Hz, CH_2N), 53.8 (NMe_2), 9.7 (C_5Me_5) ppm. ^{19}F NMR (376 MHz, CD_2Cl_2): δ = –152.4 (s) ppm. ^{195}Pt NMR (64.5 MHz, CD_2Cl_2): δ = –3115.8 ppm. ^{195}Pt NMR (64.5 MHz, acetone): δ = –3096.8 ppm. MALDI-TOF: *m*/*z* calcd. for [M – BF$_4$]$^+$ 734.14; found 733.97; calcd. C 40.96, H 4.67, N 3.41; found C 40.97, H 4.62, N 3.38.

Compound [5$_A$](BF$_4$): Compound **11** (61 mg, 116 μmol) was weighed in a dry Schlenk flask and put under inert atmosphere. A solution of [RuCp*(MeCN)$_3$](BF$_4$) (52 mg, 116 μmol) in dry dichloromethane (5 mL) was added, and the mixture stirred under nitrogen at room temperature for 2 d. The crude solution ([**5**$_A$]$^+$/[**5**$_B$]$^+$ = 7:1 by ^{1}H NMR spectroscopy) was put on top of a 50 mL silica gel column and eluted with CH_2Cl_2 that contained 1–5% (v/v) methanol. Yield: 63 mg (66%) of [**5**$_A$](BF$_4$) as a whitish powder. ^{1}H NMR (400 MHz, [D$_6$]acetone): δ = 6.68 (s, 2 H, m), 6.01 (d, 3 H, m′ + p′), 5.92 (s, 2 H, o′), 4.06 (t, $J_{H,Pt}$ = 21.5 Hz, 4 H, CH_2N), 3.03 (t, $J_{H,Pt}$ = 17.8 Hz, 12 H, NMe_2), 2.88 (s, 15 H, C_5Me_5), 2.81 and 2.73 (m, 2×2 H, C_2H_4) ppm. ^{13}C NMR (100 MHz, acetone): δ = 144.8 (*ipso*), 135.3 (o), 120.2 (p), 104.7 (i′), 97.0 (C_5R_5), 88.8, 88.3, 87.7 (o′, m′, p′), 78.3 (CH_2N), 54.5 (NMe_2), 39.0 (CH_2), 35.9 (CH_2'), 10.6 (C_5Me_5) ppm. ^{19}F NMR (376 MHz, [D$_6$]acetone): δ = –146.8 (s) ppm. ^{195}Pt NMR (64.5 MHz, [D$_6$]acetone): δ = –3170.3 ppm. MALDI-TOF: *m*/*z* calcd. for [M – BF$_4$]$^+$ 762.17; found 762.37; calcd. C 42.44, H 4.99, N 3.30; found C 42.31, H 4.96, N 3.24.

X-ray Crystallography: A solution of the complex in dichloromethane (ca. 5 to 10 mg in 1 mL) was put in an open small vial (ca. 2 mL) that was contained in a closed larger vial (ca. 20 mL). The larger vial contained about 6 mL of countersolvent. As vapor diffusion took place, crystal growth occurred at room temperature without any additional effort and crystals appeared at the bottom of the smaller vial after two to four days from pentane and one to two weeks from hexane. Crystals of [**4**$_A$]$^+$ seem to grow better from dichloromethane with hexane, whereas crystals of [**5**$_A$]$^+$ seem to grow better from dichloromethane with pentane.

Data Acquisition and Structure Refinement: All reflection intensities were measured with a Nonius Kappa CCD diffractometer (rotating anode) with graphite-monochromated Mo-K$_\alpha$ radiation (λ = 0.71073 Å) under the program COLLECT.[57] The program PEAKREF[58] was used to refine the cell dimensions. Data reduction was done with the program EVALCCD.[59] The structure was solved with the program DIRDIF99[60] and was refined on F^2 with SHELXL-97.[61] The temperature of the data collection was controlled with the OXFORD CRYOSTREAM 600 (manufactured by OXFORD CRYOSYSTEMS) system. The hydrogen atoms were placed at calculated positions (AFIX 23 or AFIX 43 or AFIX 137) with isotropic displacement parameters that had values 1.2 or 1.5 times U_{eq} of the attached C atom. Structure validation was done with PLATON[62] and illustrations were done either with MERCURY[63] or PLATON.

Compound [4$_A$](BF$_4$): $C_{28}H_{38}ClN_2PtRu{\cdot}BF_4$, M_r = 821.02; colorless needle; 0.60×0.06×0.06 mm^3; triclinic; $P\bar{1}$ (no. 2); *a* = 14.3022(4) Å, *b* = 14.7106(4) Å, *c* = 16.1515(6) Å; α = 78.021(1)°, β = 77.768(1)°, γ = 63.320(2)°; *V* = 2942.74(17) Å^3; *Z* = 4; D_{calcd} = 1.853 g cm^{-3}; μ = 5.40 mm^{-1}; 46371 reflections were measured at 150(2) K after the crystal had been flash-cooled from room temperature. Crystals are nonmerohedrally twinned and the two twin components are related by a twofold axis along [–1 1 0]. The program DIRAX[64] was used to determine the twin relationship. The minor twin fraction refines to 0.487 (2). An analytical absorption correction was based on the crystal description using the program EUHEDRAL:[65] T_{min} = 0.52 and T_{max} = 0.89; 10962 reflections were unique (R_{int} = 0.067), of which 9402 were observed with the criterion of $I > 2\sigma(I)$; 784 parameters were refined with 236 least-squares restraints. *R*1/*wR*2[$I > 2\sigma(I)$]: 0.046/0.126. *R*1/*wR*2[all refl.]: 0.058/0.138. *S* = 1.11. The residual electron density was found between –2.51 and 3.94 e Å^{-3}. Occupancy factors for the major components of the disordered counteranions: 0.66 (3) and 0.51 (1).

Compound [5$_A$](BF$_4$): $C_{30}H_{42}ClN_2PtRu.BF_4$, M_r = 849.08; colorless plate; 0.54×0.42×0.06 mm^3; orthorhombic; $P2_12_12_1$ (no. 19); *a* = 15.5374(5) Å, *b* = 17.3412(4) Å, *c* = 23.1756(6) Å; *V* = 6244.4 (3) Å^3; *Z* = 8; D_{calcd} = 1.806 g cm^{-3}; μ = 5.09 mm^{-1}; 68268 reflections were measured at 150(2) K after the crystal had been flash-cooled from room temperature. Multiscan empirical absorption corrections were applied to the data using the program SADABS:[66] T_{min} = 0.064 and T_{max} = 0.734; 14335 reflections were unique (R_{int} = 0.059), of which 11798 were observed with the criterion of $I > 2\sigma(I)$; 849 parameters were refined with 281 least-squares restraints. *R*1/*wR*2[$I > 2\sigma(I)$]: 0.039/0.073. *R*1/*wR*2[all refl.]: 0.061/0.080. *S* = 1.07. The residual electron density was found between –1.07 and 2.60 e Å^{-3}. Flack parameter: –0.016 (5).[67] Occupancy factor for the major component of the disordered Cp* ligand: 0.54(1). Occupancy factors for the major components of the disordered counter anions: 0.74(2) and 0.55(3).

DFT Calculation: All calculations were realized using B3LYP/LANL2DZ as implemented in the GAMESS-UK program.[41] The cations [**2**]$^+$–[**5**$_A$]$^+$ were minimized first using the geometry determined by X-ray crystallography as a starting point, tight convergence criteria (10^{-4} on energy), and the high-quadrature option. Chloride counteranions were added to the minimized cations so as to be able to compare neutral bimetallic species [**2**](Cl)–[**5**$_A$](Cl) to their precursor, **1**. The dipole moments indicated in Table 3 were calculated by removing the chloride anion from the minimized neutral structures, and doing a simple self-consistent field (SCF) calculation on the monocationic molecule.

CCDC-773989 {for **[4$_A$](BF$_4$)**} and -773990 {for **[5$_A$](BF$_4$)**} contain the supplementary crystallographic data for this paper. These data can be obtained free of charge from The Cambridge Crystallographic Data Centre via www.ccdc.cam.ac.uk/data_request/cif.

Supporting Information (see also the footnote on the first page of this article): Description of the packing in the X-ray structures of **[4$_A$](BF$_4$)** and **[5$_A$](BF$_4$)**. UV/Vis data for complexes **1**, [**2**]$^+$–[**5**$_A$]$^+$; picture and *x*,*y*,*z* coordinates of the DFT-minimized structures for **1** and [**2**](Cl)–[**5**](Cl); input file for DFT calculations.

Acknowledgments

We gratefully acknowledge the support of this research by Utrecht University. This work was supported in part (M. L., M. S., A. L. S.) by the Council for the Chemical Sciences of The Netherlands Organization for Scientific Research (CW- NWO). We thank the Stichting Nationale Computerfaciliteiten (National Computing Facilities Foundation, NCF) for providing supercomputer facilities.

[1] A. Ceccon, S. Santi, L. Orian, A. Bisello, *Coord. Chem. Rev.* **2004**, *248*, 683–724.
[2] J.-P. Launay, *Chem. Soc. Rev.* **2001**, *30*, 386–397.
[3] F. Paul, C. Lapinte, *Coord. Chem. Rev.* **1998**, *178*, 431–509.
[4] S. Barlow, D. O'Hare, *Chem. Rev.* **1997**, *97*, 637–669.
[5] W. D. Harman, H. Taube, *J. Am. Chem. Soc.* **1987**, *109*, 1883–1885.
[6] M. B. Sponsler, *Organometallics* **1995**, *14*, 1920–1927.
[7] J. E. Sutton, H. Taube, *Inorg. Chem.* **1981**, *20*, 3126–3134.
[8] R. Dembinski, T. Bartik, B. Bartik, M. Jaeger, J. Gladysz, *J. Am. Chem. Soc.* **2000**, *122*, 810–822.
[9] J. A. Thomas, C. J. Jones, J. A. McCleverty, D. Collison, F. E. Mabbs, C. J. Harding, M. G. Hutchings, *J. Chem. Soc., Chem. Commun.* **1992**, 1796–1798.
[10] S. H. Liu, Q. Y. Hu, P. Xue, T. B. Wen, I. D. Williams, G. C. Jia, *Organometallics* **2005**, *24*, 769–772.
[11] B. A. Etzenhouser, Q. Chen, M. B. Sponsler, *Organometallics* **1994**, *13*, 4176–4178.
[12] P. Belanzoni, N. Re, A. Sgamellotti, C. Floriani, *J. Chem. Soc., Dalton Trans.* **1998**, 1825–1835.
[13] M. Sato, Y. Kubota, Y. Kawata, T. Fujihara, K. Unoura, A. Oyama, *Chem. Eur. J.* **2006**, *12*, 2282–2292.
[14] M. Brady, W. Weng, Y. Zhou, J. Seyler, A. Amoroso, A. Arif, M. Bohme, G. Frenking, J. Gladysz, *J. Am. Chem. Soc.* **1997**, *119*, 775–788.
[15] P. J. Fagan, M. D. Ward, J. C. Calabrese, *J. Am. Chem. Soc.* **1989**, *111*, 1698–1719.
[16] M. Haga, T. Ano, K. Kano, S. Yamabe, *Inorg. Chem.* **1991**, *30*, 3843–3849.
[17] C. Cameron, P. Pickup, *J. Am. Chem. Soc.* **1999**, *121*, 11773–11779.
[18] M. C. Lagunas, R. A. Gossage, A. L. Spek, G. van Koten, *Organometallics* **1998**, *17*, 731–741.
[19] M. Gagliardo, C. H. M. Amijs, M. Lutz, A. L. Spek, R. W. A. Havenith, F. Hartl, G. P. M. van Klink, G. van Koten, *Inorg. Chem.* **2007**, *46*, 11133–11144.
[20] L. Medei, L. Orian, O. V. Semeikin, M. G. Peterleitner, N. A. Ustynyuk, S. Santi, C. Durante, A. Ricci, C. Lo Sterzo, *Eur. J. Inorg. Chem.* **2006**, 2582–2597.
[21] H. Lang, R. Packheiser, B. Walfort, *Organometallics* **2006**, *25*, 1836–1850.
[22] M. Lacoste, H. Rabaa, D. Astruc, N. Ardoin, F. Varret, J. Y. Saillard, A. Lebeuze, *J. Am. Chem. Soc.* **1990**, *112*, 9548–9557.
[23] E. J. Farrington, E. M. Viviente, B. S. Williams, G. van Koten, J. M. Brown, *Chem. Commun.* **2002**, 308–309.
[24] A. A. Koridze, A. M. Sheloumov, S. A. Kuklin, V. Y. Lagunova, I. I. Petukhova, F. M. Dolgushin, M. G. Ezernitskaya, P. V. Petrovskii, A. A. Macharashvili, R. V. Chedia, *Russ. Chem. Bull.* **2002**, *51*, 1077–1078.
[25] S. Kocher, G. P. M. van Klink, G. van Koten, H. Lang, *J. Organomet. Chem.* **2003**, *684*, 230–234.
[26] K. Kowalski, M. Linseis, R. F. Winter, M. Zabel, S. Zalis, H. Kelm, H.-J. Krueger, B. Sarkar, W. Kaim, *Organometallics* **2009**, *28*, 4196–4209.
[27] S. Bonnet, M. Lutz, A. L. Spek, G. van Koten, R. J. M. Klein Gebbink, *Organometallics* **2008**, *27*, 159–162.
[28] B. M. Trost, C. M. Older, *Organometallics* **2002**, *21*, 2544–2546.
[29] S. Bonnet, J. H. van Lenthe, M. Siegler, A. L. Spek, G. van Koten, R. J. M. Klein Gebbink, *Organometallics* **2009**, *28*, 2325–2333.
[30] S. Bonnet, J. Li, M. A. Siegler, L. S. von Chrzanowski, A. L. Spek, G. van Koten, R. J. M. Klein Gebbink, *Chem. Eur. J.* **2009**, *15*, 3340–3343.
[31] G. Rodriguez, M. Albrecht, J. Schoenmaker, A. Ford, M. Lutz, A. L. Spek, G. van Koten, *J. Am. Chem. Soc.* **2002**, *124*, 5127–5138.
[32] For example in the reaction between $[Ru(C_5H_5)(MeCN)_3]^+$ and complex **8** the A/B ratio is 0.79.
[33] B. Chaudret, X. He, Y. Huang, *J. Chem. Soc., Chem. Commun.* **1989**, 1844–1846.
[34] E. Rüba, K. Mereiter, K. M. Soldouzi, C. Gemel, R. Schmid, K. Kirchner, *Organometallics* **2000**, *19*, 5384–5391.
[35] X. D. He, B. Chaudret, F. Dahan, Y.-S. Huang, *Organometallics* **1991**, *10*, 970–979.
[36] M. Q. Slagt, G. Rodriguez, M. M. P. Grutters, R. J. M. Klein Gebbink, W. Klopper, L. W. Jenneskens, M. Lutz, A. L. Spek, G. van Koten, *Chem. Eur. J.* **2004**, *10*, 1331–1344.
[37] M. Gagliardo, D. J. M. Snelders, P. A. Chase, R. J. M. Klein Gebbink, G. R. M. van Klink, G. van Koten, *Angew. Chem. Int. Ed.* **2007**, *46*, 8558–8573.
[38] H. Jude, J. A. K. Bauer, W. B. Connick, *Inorg. Chem.* **2004**, *43*, 725–733.
[39] S. Back, R. A. Gossage, M. Lutz, I. del Rio, A. L. Spek, H. Lang, G. van Koten, *Organometallics* **2000**, *19*, 3296–3304.
[40] S. Back, M. Lutz, A. L. Spek, H. Lang, G. van Koten, *J. Organomet. Chem.* **2001**, *620*, 227–234.
[41] M. F. Guest, I. J. Bush, H. J. J. van Dam, P. Sherwood, J. M. H. Thomas, J. H. van Lenthe, R. W. A. Havenith, J. Kendrick, *Mol. Phys.* **2005**, *103*, 719–747.
[42] The DFT-minimized structure of complex **1** has recently been published by our group using B3LYP/LANL2DZ as implemented in Gaussian98 (see ref.[36]). For homogeneity reasons we repeated the calculation using GAMESS-UK, and both programs give the same geometry. However, a systematic error in reporting the natural population analysis (NPA) charges on Pt made them twice too low (ca. 0.3) in Slagt's original publication; this does not, however, change the general conclusions of the paper. We report here the correct NPA charges (ca. 0.6).
[43] A. E. Reed, L. A. Curtiss, F. Weinhold, *Chem. Rev.* **1988**, *88*, 899–926.
[44] O. G. Stradella, H. O. Villar, E. A. Castro, *Theor. Chim. Acta* **1986**, *70*, 67–71.
[45] R. S. Mulliken, *J. Chem. Phys.* **1955**, *23*, 1833–1840.
[46] M. D. Gould, C. Taylor, S. K. Wolff, G. S. Chandler, D. Jayatilaka, *Theor. Chem. Acc.* **2008**, *119*, 275–290.
[47] M. Hirasa, A. Inagaki, M. Akita, *J. Organomet. Chem.* **2007**, *692*, 93–110.
[48] D. E. Wheeler, S. T. Hill, J. M. Carey, *Inorg. Chim. Acta* **1996**, *249*, 157–161.
[49] G. D. Batema, K. T. L. van de Westelaken, J. Guerra, M. Lutz, A. L. Spek, C. A. van Walree, C. D. Donega, A. Meijerink, G. P. M. van Klink, G. van Koten, *Eur. J. Inorg. Chem.* **2007**, 1422–1435.
[50] M. A. Siegler, S. Bonnet, A. M. M. Schreurs, R. J. M. Klein Gebbink, G. van Koten, A. L. Spek, *J. Chem. Crystallogr.* **2010**, 40, 753–760.
[51] M. Albrecht, M. Lutz, A. M. M. Schreurs, E. T. H. Lutz, A. L. Spek, G. van Koten, *J. Chem. Soc., Dalton Trans.* **2000**, 3797–3804.
[52] Opposite effects had been obtained upon attaching the NCN-pincer metal fragment to ferrocene: in such a case, oxidation of the pincer metal center was easier due to the negative charge of the *para*-Cp ligand η^5-coordinated to iron(II). See: B. Kocher, B. Walfort, G. P. M. van Klink, G. van Koten, H. Lang, *J. Organomet. Chem.* **2006**, *691*, 3955–3961.
[53] A. Fürstner, P. W. Davies, *Angew. Chem. Int. Ed.* **2007**, *46*, 3410–3449.
[54] P. Steenwinkel, S. L. James, D. M. Grove, N. Veldman, A. L. Spek, G. van Koten, *Chem. Eur. J.* **1996**, *2*, 1440–1445.

[55] J. Terheijden, G. van Koten, W. P. Mul, D. J. Stufkens, F. Muller, C. H. Stam, *Organometallics* **1986**, *5*, 519–525.
[56] A. A. H. van der Zeijden, G. van Koten, R. A. Nordemann, B. Kojicprodic, A. L. Spek, *Organometallics* **1988**, *7*, 1957–1966.
[57] B. V. Nonius, in: *COLLECT*, Delft, The Netherlands, **1998**.
[58] A. M. M. Schreurs, in: *PEAKREF*, Utrecht University, Utrecht, The Netherlands, **2005**.
[59] A. J. M. Duisenberg, L. M. J. Kroon-Batenburg, A. M. M. Schreurs, *J. Appl. Crystallogr.* **2003**, *36*, 220.
[60] P. T. Beurskens, G. Admiraal, G. Beurskens, W. P. Bosman, S. Carcia-Granda, R. O. Gould, J. M. M. Smits, C. Smykalla in *The DIRDIFF99 Program System, Technical Report of the Crystallography Laboratory*, University of Nijmegen, Nijmegen, The Netherlands, **1999**.
[61] G. M. Sheldrick, *SHELXL97*, University of Göttingen, Göttingen, Germany, **1997**.
[62] A. L. Spek, *J. Appl. Crystallogr.* **2003**, *36*, 7–13.
[63] C. F. Macrae, P. R. Edgington, P. McCabe, E. Pidcock, G. P. Shields, R. Taylor, M. Towler, J. van De Streek, *J. Appl. Crystallogr.* **2006**, *39*, 453–457.
[64] A. J. M. Duisenberg, *J. Appl. Crystallogr.* **1992**, *25*, 92–96.
[65] M. Lutz, A. M. M. Schreurs, *EUHEDRAL*, Utrecht, The Netherlands, **2001**.
[66] G. M. Sheldrick, *SADABS*, Göttingen, Germany, **2003**.
[67] H. D. Flack, *Acta Crystallogr., Sect. A* **1983**, *39*, 876–881.

Received: April 22, 2010
Published Online: August 18, 2010

